Design, Optimization, and Experimental Validation of a 3-DOF Parallel Robotic Ankle Based on a 2SPU-1RU Architecture

Gonzalo Oshiro[1]; Brayam J. Lazares[2]; Claudia Casanova[3]; Victoria E. Abarca[4] and Dante A. Elias[5]

Abstract— **This paper presents the design, implementation, and experimental validation of a 3-degree-of-freedom (3-DOF) parallel robotic ankle based on a 2SPU-1RU (two Spherical-Prismatic-Universal kinematic chains and one Revolute-Universal kinematic chain) architecture for transtibial prosthesis applications. The proposed design aims to replicate the complex kinematics of the human ankle across the sagittal, frontal, and transverse planes, addressing the limitations of conventional prosthetic ankles, which typically offer reduced mobility. The system was developed in accordance with ISO 10328:2016 load requirements (P4 level) and incorporates a parallel mechanism that enhances structural rigidity. A comprehensive methodology, including CAD modeling, kinematic simulation, finite element analysis (FEA), and electronic system integration, was implemented. Structural analysis results showed a maximum Von Mises stress of 193.2 MPa and a safety factor of 2.17, ensuring operation within elastic limits. The prototype, fabricated using 3D printing (PLA), integrates linear actuators, a servomotor, and a sensing system with closed-loop PID control. Experimental validation under no-load conditions demonstrated that the system achieved clinically relevant ranges of motion, including 41.0° of plantarflexion, 16.5° of dorsiflexion, 26.1° of inversion, and 12.4° of eversion. The maximum angular deviation with respect to target values was 3.5°, confirming high kinematic fidelity. These results show the feasibility of the 2SPU-1RU configuration as a compact, efficient solution for advanced ankle prostheses, with potential for future integration into functional assistive devices.**

I. INTRODUCTION

Amputation results in permanent disability and profoundly affects the lifestyle of the person who undergoes it [1]. Of all amputations performed, lower limb amputation is the most common, and within this group, transtibial amputation has a prevalence of 80% [2]. The main causes of transtibial amputation are vascular diseases and diabetes-related complications [3]. Peripheral arterial disease leads to partial or total vascular occlusion, which can progress from intermittent claudication to arterial ulceration, rest ischemia, and limb loss [4]. People with diabetes-related complications face a 30-fold increased risk of amputation compared to those without the disease [5].

The literature shows that amputation affects physical and psychological well-being, leading to significant changes in a person's life [6]. A systematic review of 52 studies on lower-limb amputees identified the main areas affected as mobility, participation in social activities, the possibility of returning to work, and emotional well-being [7]. Psychologically, perceived confidence in balance decreases, and the risk of depression and anxiety increases [8]. Research has shown that physical activity provides meaningful benefits for the physical and mental health of people with transtibial amputations [9]. It is therefore essential that these individuals regain the ability to walk effectively across diverse environments, on various surfaces, and in situations requiring agility.

As a result, there is a growing demand for advanced prosthetic technologies that improve balance and stability during gait [10]. The ankle joint performs movements in all three anatomical planes: plantar flexion and dorsiflexion in the sagittal plane, adduction and abduction in the transverse plane, and inversion and eversion in the frontal plane [11]. However, currently available commercial ankle prostheses can only perform one-degree-of-freedom movement within a limited range [12], [13]. Several attempts have been made to develop a powered 2-degree-of-freedom (2-DoF) ankle-foot prosthesis. Bellman et al. proposed a mechanical design for a high-power 2-DoF ankle capable of performing tasks equivalent to those of a human ankle [14]; however, its large size and weight limit its practical application [15]. Hsieh et al. proposed an untethered 2-DoF ankle prosthesis [15]; nevertheless, it has been validated only on level ground for users weighing around 77 kg, and transverse-plane movement was not addressed. A 2SPU-RU parallel mechanism was also proposed, incorporating three active degrees of freedom to replicate ankle movement across the three anatomical planes [16]. The advantages of parallel mechanisms include high structural rigidity with reduced sensitivity to external disturbances, improved dynamic response and movement repeatability, and a compact design that allows for a greater workspace [17].

This study presents a mechanical optimization of the transtibial prosthesis prototype based on the 2SPU-RU (two Spherical-Prismatic-Universal kinematic chains and one Revolute-Universal kinematic chain) parallel mechanism developed by Abarca et al. [16]. A three-degree-of-freedom robotic ankle joint mechanism is proposed for integration as

*This work is supported by The National Program for Scientific Research and Advanced Studies (PROCIENCIA-CONCYTEC), under contract No. PE501086900-2024-PROCIENCIA.

[1]Gonzalo Oshiro, Biomechanics and Applied Robotics Research Laboratory, Pontificia Universidad Católica del Perú, 15088 Lima, Perú. gonzalo.oshiro@pucp.edu.pe

[2]Brayam J. Lazares, Biomechanics and Applied Robotics Research Laboratory, Pontificia Universidad Católica del Perú, 15088 Lima, Perú. brayam.lazares@pucp.edu.pe

[3]Claudia Casanova, Biomechanics and Applied Robotics Research Laboratory, Pontificia Universidad Católica del Perú, 15088 Lima, Perú. claudia.casanova@pucp.edu.pe

[4]Victoria E. Abarca, Biomechanics and Applied Robotics Research Laboratory, Pontificia Universidad Católica del Perú, 15088 Lima, Perú. victoria.abarca@pucp.edu.pe

[5]Dante A. Elias, Biomechanics and Applied Robotics Research Laboratory, Pontificia Universidad Católica del Perú, 15088 Lima, Perú. delias@pucp.pe

an articular component in a transtibial prosthesis. Compared to [16], the proposed design incorporates enhanced actuation and sensing capabilities, closed-loop PID control with potentiometer-based feedback, and a multi-level validation framework combining finite element analysis under ISO 10328:2016 (P4-80kg) with experimental kinematic verification. Moreover, the design addresses all three anatomical planes, including adduction and abduction, which are among the least reported motions in the active prosthesis literature, and incorporates a prosthetic foot with a plantar arch and an elastic plantar fascia element validated under ISO 22675 category P5 [18].

II. MATERIALS AND METHODS

A. Mechanical Design

1) Requirements: The system must comply with the load conditions specified in ISO 10328:2016, level P4, for users up to 80 kg, including peak loading at heel-strike and toe-off, while limiting permanent deformation to less than 5 mm. Additionally, the structure must maintain a functional height of 45-55 cm to ensure compatibility with transtibial prosthetic configurations. From a kinematic standpoint, the system must achieve the following ranges of motion: 40° plantar flexion, 20° dorsal flexion, 12° eversion, 23° inversion, and ±15° abduction-adduction.

2) CAD Modeling: The robotic ankle prototype was designed in Autodesk Inventor as a multiaxial configuration. The architecture integrates spherical and universal joints alongside linear and rotational actuators to reproduce the complex kinematics of the human ankle. The design was dimensioned to meet the structural load requirements of level P4 as defined in ISO 10328:2016, ensuring that stress and deformation values remain within admissible limits. The structure is sized to a functional height of 45–55 cm.

3) Kinematics and Range of Motion: The system exhibits multiple degrees of freedom distributed across three kinematic chains: two chains composed of a proximal spherical joint, a distal universal joint, and an interconnecting linear actuator, and a third chain integrating a distal universal joint and a proximal servomotor. Kinematic simulations were used to verify the range of motion in the primary anatomical planes. In the sagittal plane, the system reaches 40° of plantarflexion and 21° of dorsiflexion. In the transverse plane, it achieves 33° of adduction and 30° of abduction.

4) Structural Analysis: The structural analysis followed the static test guidelines defined in ISO 10328:2016, implemented as a linear static finite element analysis (FEA). The simulations were performed using SimScale. Loading Conditions I and II were evaluated at maximum dorsiflexion (21°) and maximum plantarflexion (40°), respectively, as these configurations maximize the moment arm between the applied load vector and the proximal constraint for each condition, as shown in Fig. 1.

The proximal auxiliary component was modeled as a fixed constraint. Contacts between components were defined as ideal rigid bonded joints, representing a conservative assumption of structural continuity.

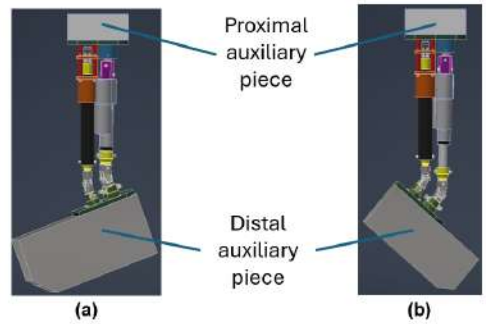

Fig. 1. Auxiliary components and loading configurations: (a) Condition I, (b) Condition II

Commercial components, such as universal and spherical joints, were modeled using AISI 52100 steel. Auxiliary components, distal and proximal, were modeled as high-strength steel with a Young's modulus of 207 GPa. The remaining structural elements were evaluated using Aluminum 6061-T6 as a reference material. While this material assignment represents the intended final fabrication, the current physical prototype was manufactured in PL solely for kinematic and assembly validation.

The mesh was discretized with tetrahedral elements of average size 0.7 mm and minimum size 0.02 mm, with local refinement applied at fillets and inter-component interfaces.

5) Stress and Deformation Evaluation: Results show a maximum Von Mises stress of 193.2 MPa, localized at the rotation points of the universal joint. The maximum deformation was 0.48 mm, occurring at the Universal-Head component. Considering a yield strength of 420 MPa for the universal joint material, the minimum safety factor obtained is 2.17, as shown in Fig. 2.

All deformations remain within the elastic regime of the respective materials; therefore, no permanent deformation is expected under the evaluated loading conditions.

B. Electronic Design

The electronic architecture of the 2SPU-1RU robotic ankle integrates computing, communication, actuation, sensing, and power subsystems, as shown in Fig. 3.

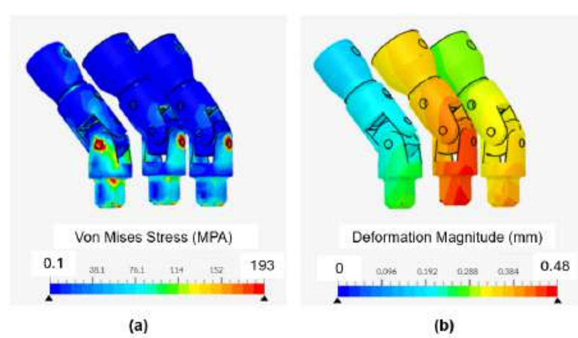

Fig. 2. Static analysis of the robotic ankle's critical components shows Von Mises stress distribution (a) concentrated at the universal joint axes, and deformation (b) localized at the distal region, known as Universal-Head.

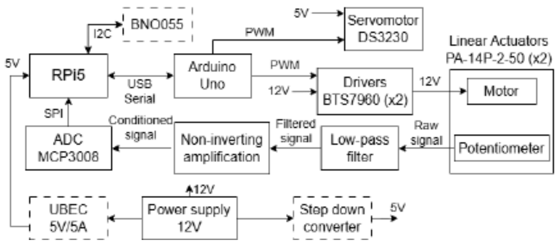

Fig. 3. Electronic architecture of the 2SPU-1RU robotic ankle prototype. Dashed blocks indicate components provisioned for future implementation.

1) Computing and Communication: A Raspberry Pi 5 (RPi5) serves as the main computing unit and high-level controller. It executes the position-control algorithm and communicates with a subordinate Arduino Uno microcontroller via USB-Serial. At each control cycle, the RPi5 transmits a command array containing the target angle for the servomotor and the PWM duty cycle values for each linear actuator. The Arduino Uno receives these commands and generates the corresponding PWM signals to drive the actuators.

2) Actuation Subsystem: The prototype employs three actuators consistent with its 2SPU-1RU kinematic structure. The two SPU chains are actuated by Progressive Automation PA-14P-2-50 electric linear actuators, driven by BTS7960 H-bridge modules operating at 12 VDC. The polarity of the PWM command determines motion direction extension or retraction, while the duty cycle magnitude governs actuation speed. The RU chain is actuated by a DS3230 digital servomotor operating at 5 VDC, which features an integrated controller that accepts a standard PWM position signal directly from the Arduino Uno.

3) Sensing Subsystem: Each linear actuator integrates a 10 kΩ linear potentiometer for position feedback. The raw potentiometer signal was found to be noisy and to underutilize the ADC input range; therefore, a dedicated signal conditioning stage was implemented. It consists of a first-order RC low-pass filter with a cutoff frequency of 159.15 Hz, followed by a non-inverting amplifier stage built around an LM324N operational amplifier. The conditioned signals are digitized by an MCP3008 8-channel, 10-bit ADC, which communicates with the RPi5 via the SPI protocol. The system also incorporates a BNO055 IMU, which is provisioned for future gait-intention detection.

4) Power Subsystem: The linear actuators are powered at 12 VDC, the Arduino Uno and DS3230 servomotor at 5 VDC, and the RPi5 via USB-C. The system design includes DC-DC step-down converters to enable self-contained portable operation. During the current validation phase, a regulated bench power supply is used in place of the onboard converters.

C. Implementation

1) Fabrication: The prototype was fabricated primarily using fused deposition modeling (FDM) 3D printing with polylactic acid (PLA), as shown in Fig. 4. Printed components include the fixed base, the moving platform, the universal joint connectors, the linear actuator-to-cardan linkages, the spherical joint housings, the servomotor housing, and the shaft connecting the servomotor to the moving platform. Most parts were printed at 15% infill density; the actuator-to-cardan linkage was reinforced to 60% infill following structural failure observed during preliminary testing. Non-printed components include linear actuators, the servomotor, cardan joints, spherical joints, flexible couplings, bearings, and standard fasteners (M4, M5, and M6 bolts and nuts).

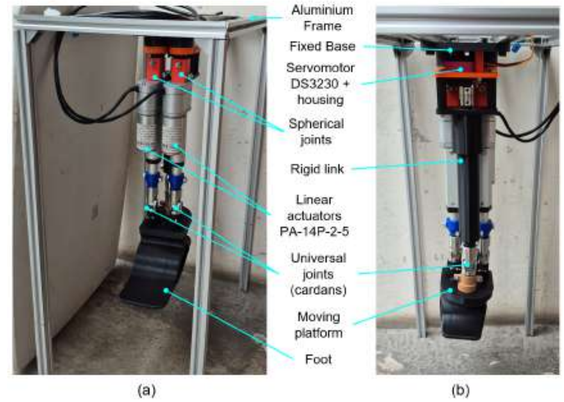

Fig. 4. Assembled 2SPU-1RU robotic ankle prototype: (a) front view, (b) rear view.

The overall prototype dimensions are 120 mm × 240 mm × 460 mm (width × depth × height), with a total assembled mass of 3.8 kg.

A significant mass fraction is concentrated in off-the-shelf functional components: the two linear actuators (1.72 kg) and three steel universal cardan joints (0.46 kg), selected to prioritize mechanical robustness and availability. Although this exceeds the mass of passive prosthetic ankles (0.5–1.5 kg), powered ankle-foot devices have been shown to partially offset metabolic cost through active energy contribution [19].

2) Comparison with Previous Prototype: A quantitative comparison with the previous prototype [16], is shown in Table I.

3) Assembly: Components are assembled using standard metric fasteners. Actuator rods are secured to spherical bearings using retaining springs, and the motor shaft is coupled to the universal joint via a flexible coupling with a retaining piece designed to prevent decoupling during rotation, following an issue identified during initial assembly trials. During functional testing, slippage between the servomotor shaft and the flexible coupling was identified, preventing effective torque transmission to the moving platform. A redesign of the shaft-coupling interface is currently underway as part of ongoing development.

D. Experimental Protocol

Functional validation of the integrated prototype was performed using a rigid support frame constructed from aluminum extrusion profiles measuring 31 cm × 52 cm × 72 cm (width × length × height). The prototype was suspended

TABLE I

COMPARISON OF ANKLE PROSTHESIS PROTOTYPES

Feature	Hsieh [15]	Ficanha [19]	Rogers [22]	Abarca [16]	This work
Architecture[DoF[1]]	Serial[2]	Parallel[2]	2PU Parallel[2]	2SPU-RU Parallel[3]	2SPU-1RU Parallel[3]
Planes validated	Sag.	Sag., Front.	Sag., Front.	Sag., Front., Trans. (sim.)	Sag., Front.
Actuators	2 Rotational: 40 N·m	2 Rotational: 256 N·m	2 Rotational: 1N·m	Lineal: 90N Rotational: 0.3 kg·cm	Lineal: 222N Rotational: 30 kg·cm
Control	Impedance + FSM[2]	PD position; strain-gage feedback	EMG[3] + dyn. joint model PID; FSM[2] 2-state	On-Off	Closed-loop PID
Structural validation	No	No	FEA[5]	No	FEA[5] (SF[5] = 2.17)
Plantar/Dorsal flexion	21°/9°	22°/—	14.3°/4.0°	13°/24°	41.0°/16.5°
Eversion/Inversion	13.5°/13.5°	—/20°	0.4°/4.6°	13°/26°	12.4°/26.1°
Prototype material	Al[6] 7075-T6 SS 304, Nylon PA11	Carbon Fiber, Nylon	Ti 6Al-4V; Al[6] 7075-T6 Nylon PA (3D-printed)	PLA	PLA

[1]DoF: Degrees of Freedom [2]FSM: Finite State Machine [3]EMG: Electromyography [5]FEA: Finite Element Analysis; SF: Safety Factor [6]Al: Aluminum

from the upper frame, allowing the moving platform to move freely in all directions without contacting the ground, following a methodology analogous to that used in the kinematic validation of the previous prototype [16]. All tests were performed under no-load conditions due to the low yield strength of PLA in this iteration, physical structural validation under ISO 10328 is reserved for future work.

A PID controller was implemented for closed-loop position control using potentiometer feedback. Based on the inverse kinematics model fully derived in [20], target actuator displacements are computed as (1).

$$l_i = |\mathbf{p} + \mathbf{b}_i - \mathbf{a}_i|, \quad i = 2,3 \tag{1}$$

where $\mathbf{a}_i$, $\mathbf{b}_i$ are joint positions on the fixed and moving platforms, and $\mathbf{p}$ is the position of B_1, using a Bryant–Cardan ZXY rotation sequence [20]. This model was implemented in MATLAB 2024b to compute the actuator setpoints used during validation. The control law is (2).

$$u(t) = K_p e(t) + K_i \int e(t)\,dt + K_d \frac{de}{dt} \tag{2}$$

where $e(t)$ is the stroke error in mm. Gains ($K_p = 5000$, $K_i = 10$, $K_d = 5$) were tuned heuristically: K_p for rapid response, K_i to eliminate friction-induced steady-state error, K_d to smooth transients. Actuator position was expressed in millimeters based on a calibrated ADC-to-stroke mapping. Two validation tests were performed:

1) Actuator stroke validation: Step commands were applied independently to each linear actuator to verify full-range operability. Commands were issued from the initial position of 17 mm to the minimum stroke (0 mm) and maximum stroke (50 mm), confirming actuator travel limits and the absence of mechanical interference throughout the range. Since dorsiflexion and plantarflexion result from symmetric extension and retraction of both linear actuators, full-stroke operability of each actuator implicitly validates the sagittal plane range of motion of the prototype.

2) Joint angle validation: Step commands were applied simultaneously to both actuators to achieve target inversion and eversion angles. For 23° of inversion, actuator A2 was commanded to 7.2 mm and A3 to 26.8 mm. For 12° of eversion, A2 was commanded to 22.2 mm and A3 to 11.8 mm. Joint angles were selected based on clinically reported ranges for normal gait [21]. All motion data were recorded using ROS 2 bags for post-processing and visualization. Additionally, joint angles obtained during testing were verified via video analysis in Kinovea v2023.1.2 by measuring joint orientation at representative frames corresponding to the target configurations.

III. RESULTS

Experimental validation is presented for sagittal and frontal plane motions. Transverse-plane validation could not be completed because of a mechanical limitation associated with the servomotor coupling interface, as described in Section II-C and discussed further at the end of this section.

A. Range of Motion and Actuator Stroke

Fig. 5 shows the displacement of linear actuators A2 and A3 when performing full-stroke transitions. From a neutral standing position (17 mm), the actuators were commanded to their physical limits (0 mm and 50 mm).

The experimental data confirm that the mechanism achieves a maximum extension of approximately 41° and a minimum dorsiflexion. As shown in the plots, despite the presence of low-amplitude high-frequency noise in the potentiometer feedback—attributed to the ADC sampling and mechanical vibrations—the steady-state error remains negligible ($e_{ss} < 1$ mm).

Settling time ≈2 s with no overshoot; dead time ≈1 s due to serial latency and actuator friction; $\omega_{BW} \approx 2$ rad/s and phase margin $> 65°$.

Isolated spike artifacts reflect intermittent potentiometer noise not fully attenuated by the analog stage (cutoff: 159.15 Hz), not mechanical instability. Future mitigation includes digital median filtering and optical encoders.

B. Frontal Plane Analysis: Inversion and Eversion

The 2SPU-1RU parallel mechanism achieves frontal plane motion through differential actuation. Fig. 6 shows the coordinated movement for target angles of 23° (inversion) and 12° (eversion). For the inversion test, actuator A2 retracted to 7.2 mm while A3 extended to 26.8 mm. During eversion, the behavior was reversed ($A2 = 22.2$ mm, $A3 = 11.8$ mm). The smooth transition between these states confirms that

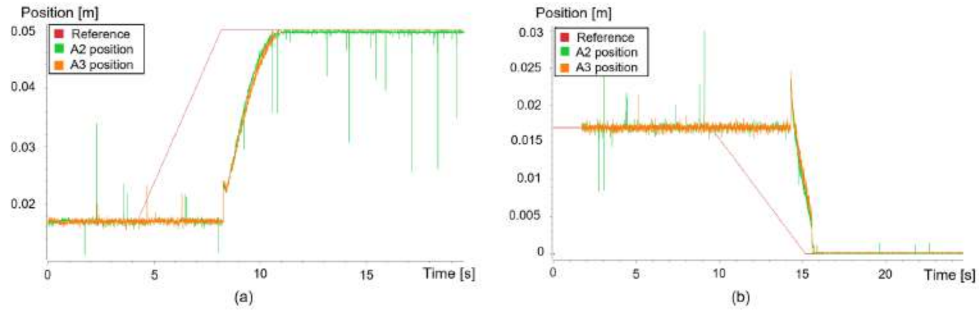

Fig. 5. Experimental position response for actuators A2 and A3: (a) transition to maximum stroke (50 mm) and (b) transition to minimum stroke (0 mm). The red line represents the reference setpoint, while green and orange lines show the measured positions for A2 and A3, respectively.

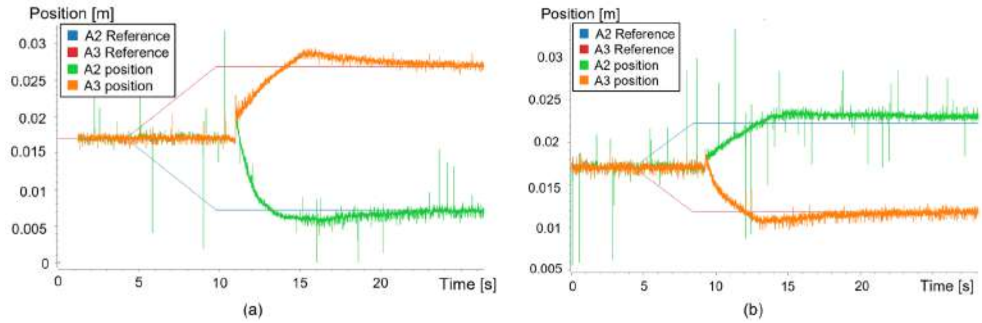

Fig. 6. Actuator position responses for frontal plane motion: (a) inversion test case (23°) and (b) eversion test case (12°). Blue and red lines represent the reference setpoints for A2 and A3, respectively, while green and orange lines show the measured positions.

the optimized joint locations and the universal joint (RU) at the base provide the necessary degrees of freedom without structural stress.

C. Visual Validation and Kinematic Accuracy

To verify the correspondence between the actuator positions and the actual joint orientation, a video analysis was performed using Kinovea v2023.1.2. This external validation ensures that the actuators' linear displacement correctly translates into the desired angular orientation of the moving platform. Fig. 7 shows the validation for the sagittal plane.

The prototype reached a maximum plantar flexion of 41.0° and a maximum dorsal flexion of 16.5°. Similarly, Fig. 8 shows the frontal plane transitions, achieving 26.1° of inversion and 12.4° eversion.

Table II summarizes target versus measured angles. The maximum deviation of 3.5° in dorsiflexion is attributed to mechanical clearance in the spherical joints, dimensional differences between the CAD model and the fabricated prototype, and the inherent uncertainty of the Kinovea-based method (±1–2°; recording conditions: 996×1770 px, 60 fps).

Experimental validation in the transverse plane could not be completed due to slippage in the servomotor shaft–coupling interface, preventing effective torque transmission. This mechanism is being redesigned; therefore, no experimental results for transverse-plane motion are reported in the manuscript.

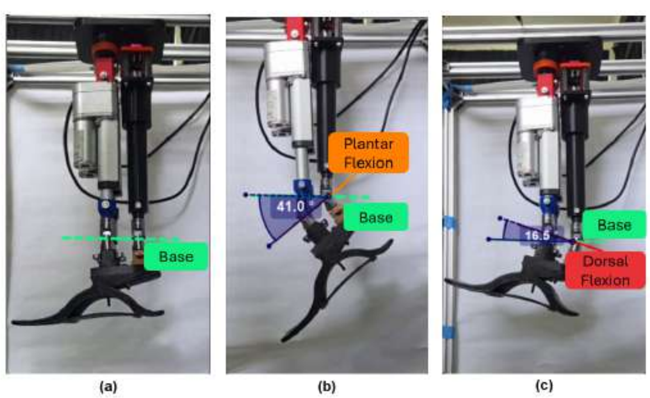

Fig. 7. Visual validation of sagittal plane motion: (a) neutral position, (b) maximum plantar flexion reached at 41.0°, and (c) maximum dorsal flexion reached at 16.5°.

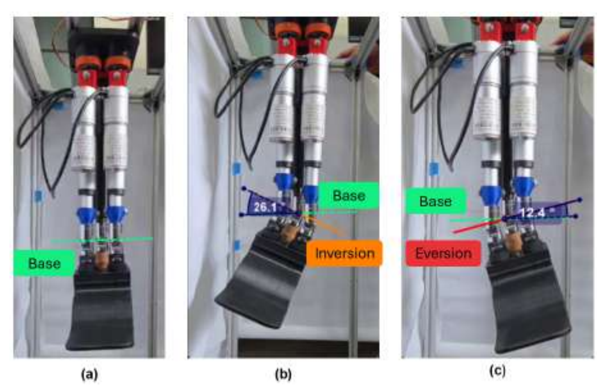

Fig. 8. Visual validation of frontal plane motion: (a) neutral position, (b) inversion at 26.1°, and (c) eversion at 12.4°.

TABLE II
COMPARISON BETWEEN TARGET AND MEASURED JOINT ANGLES

Movement	Target Angle	Measured (Video)	Error
Plantarflexion	40.0°	41.0°	1.0°
Dorsiflexion	20.0°	16.5°	3.5°
Inversion	23.0°	26.1°	3.1°
Eversion	12.0°	12.4°	0.4°

IV. CONCLUSIONS

This work presented the design, optimization, and validation of a 3-DOF parallel robotic ankle based on a 2SPU-1RU architecture for transtibial prosthetic applications. The proposed system successfully replicates the primary ankle movements across multiple anatomical planes while maintaining structural robustness and compactness.

The mechanical design, supported by finite element analysis, demonstrated adequate strength and stiffness under standardized loading conditions, achieving a safety factor greater than 2. Experimental results confirmed that the prototype reaches clinically relevant ranges of motion with acceptable accuracy, with a maximum angular deviation of 3.5°. Closed-loop PID control enabled stable and repeatable actuation, with a settling time of approximately 2 s, no overshoot, and steady-state error below 1 mm.

Compared to previous prototypes, the current system shows significant improvements in load capacity, actuation performance, and scalability toward real-world applications. Although validation was conducted under no-load conditions, the combined use of finite element analysis and experimental kinematic verification provides consistent evidence of structural integrity and motion accuracy, supporting the system's feasibility for future load-bearing evaluation. Transverse-plane validation could not be completed due to slippage in the servomotor shaft-coupling interface, which is currently being addressed.

Future work will focus on redesigning the shaft–coupling interface to ensure reliable torque transmission in the transverse plane, structural optimization using metallic materials, and incorporating gait-intention detection using IMU data.

ACKNOWLEDGMENT

The authors gratefully acknowledge the financial support provided by the Government of Peru through the National Program for Scientific Research and Advanced Studies (PROCIENCIA–CONCYTEC), under Contract No. PE501086900-2024-PROCIENCIA.

REFERENCES

[1] N. Mukkamala and S. Vala, "Functional mobility in individuals with lower limb amputation: An observational study," Cureus, Jan. 2024.

[2] A. K. P. Sathsara, K. N. D. Widanage, N. Sooriyaperakasam, R. K. P. S. Ranaweera, and R. A. R. C. Gopura, "A Hybrid Powering Mechanism for a Transtibial Robotic Prosthesis," 2019 Moratuwa Engineering Research Conference (MERCon), Moratuwa, Sri Lanka, 2019, pp. 447-453.

[3] A. F. Ying, T. Y. Tang, A. Jin, T. T. Chong, D. J. Hausenloy, and W.-P. Koh, "Diabetes and other vascular risk factors in association with the risk of lower extremity amputation in chronic limb-threatening ischemia: a prospective cohort study," Cardiovascular Diabetology, vol. 21, no. 1, Jan. 2022.

[4] F. Gul and S. F. Janzer, "Peripheral vascular disease," in *StatPearls* [Online]. Treasure Island, FL, USA: StatPearls Publishing, Jan. 2026. [Updated Jun. 6, 2023]. Available: https://www.ncbi.nlm.nih.gov/books/NBK557482/

[5] H. M. Murphy-Lavoie, A. Ramsey, M. Nguyen *et al.*, "Diabetic foot infections," in *StatPearls* [Online]. Treasure Island, FL, USA: StatPearls Publishing, Jan. 2026, updated Apr. 11, 2025. Available: https://www.ncbi.nlm.nih.gov/books/NBK441914/

[6] S. Gozaydinoglu, Z. Hosbay, and H. Durmaz, "Body image perception, compliance with a prosthesis and cognitive performance in transfemoral amputees," Acta Orthopaedica et Traumatologica Turcica, vol. 53, no. 3, pp. 221–225, May 2019.

[7] L. Calabrese, M. Maffoni, V. Torlaschi, and A. Pierobon, "What Is Hidden behind Amputation? Quanti-Qualitative Systematic Review on Psychological Adjustment and Quality of Life in Lower Limb Amputees for Non-Traumatic Reasons," Healthcare, vol. 11, no. 11, pp. 1661–1661, Jun. 2023.

[8] O. Horgan and M. MacLachlan, "Psychosocial adjustment to lower-limb amputation: A review," Disability and Rehabilitation, vol. 26, no. 14–15, pp. 837–850, Jul. 2004.

[9] J. Langford, M. P. Dillon, C. L. Granger, and C. Barr, "Physical activity participation amongst individuals with lower limb amputation," Disability and Rehabilitation, vol. 41, no. 9, pp. 1063–1070, Jan. 2018.

[10] S. Manz et al., "A review of user needs to drive the development of lower limb prostheses," Journal of NeuroEngineering and Rehabilitation, vol. 19, no. 1, Nov. 2022.

[11] M. Marco, P. Giovanni, S. Valter, and T. Lucrezia, "Total Ankle Replacement: Indications, Rehabilitation and Results," International Journal of Foot and Ankle, vol. 2, no. 2, Dec. 2018.

[12] "Ottobock" *Ottobock*, 2024. [Online]. Available: https://www.ottobock.com/en-us/product/1A1-2-61113

[13] "Proprio Foot: pie y tobillo protésicos biónicos", *Ossur*, 2026. [Online]. Available: https://www.ossur.com/es-es/protesica/pies/proprio-foot. [Accessed: Apr. 20, 2026].

[14] R. D. Bellman, M. A. Holgate, and T. G. Sugar, "SPARKy 3: Design of an active robotic ankle prosthesis with two actuated degrees of freedom using regenerative kinetics," 2008 2nd IEEE RAS & EMBS International Conference on Biomedical Robotics and Biomechatronics, Scottsdale, AZ, USA, 2008, pp. 511-516.

[15] T.-H. Hsieh et al., "Design, Characterization, and Preliminary Assessment of a Two-Degree-of-Freedom Powered Ankle–Foot Prosthesis," Biomimetics, vol. 9, no. 2, pp. 76–76, Jan. 2024.

[16] V. E. Abarca, G. Oshiro, O. A. Gonzales-Huisa, and D. A. Elias, "Design exploration and kinematic validation of a transtibial prosthesis using a 2SPU-RU parallel mechanism," Intelligent Service Robotics, vol. 18, no. 6, pp. 1315–1337, 2025.

[17] A. Todor, D. V. Banyai, C. Brisan, and A. D. Banyai, "Aspects Concerning Parallel Robots Used in Rehabilitation," Bioengineering, vol. 12, no. 11, p. 1224, Nov. 2025.

[18] M. Lagones, V. E. Abarca, and D. A. Elias, "Design and Validation of a Prosthetic Foot Adaptable to Sagittal Plane Ground Irregularity," 2024 International Symposium on 3D Analysis of Human Movement (3DAHM), Montevideo, Uruguay, 2024, pp. 1-6.

[19] E. M. Ficanha, M. Rastgaar, and K. R. Kaufman, "A Two-Axis Cable-Driven Ankle-Foot Mechanism," Journal of Robotics and Biomimetics, vol. 1, no. 1, art. 17, Nov. 2014, doi: 10.1186/s40638-014-0017-0.

[20] V. E. Abarca and D. A. Elias, "Modeling and Simulation of a 2SPU-RU Parallel Mechanism for a Prosthetic Ankle with Three Degrees of Freedom," Inventions, vol. 9, no. 4, p. 71, Jul. 2024, doi: 10.3390/inventions9040071.

[21] C. L. Brockett y G. J. Chapman, "Biomechanics of the ankle", Orthop. Trauma, vol. 30, núm. 3, pp. 232–238, 2016.

[22] E. A. Rogers, T. Goan, and A. M. Gardinier, "An Ankle-Foot Prosthesis for Rock Climbing Augmentation," IEEE Trans. Neural Syst. Rehabil. Eng., vol. 29, pp. 41–51, 2021, doi: 10.1109/TNSRE.2020.3033474.